Available online at www.sciencedirect.com
ScienceDirect
Polymer 48 (2007) 3703–3716
polymer
www.elsevier.com/locate/polymer

A study by Raman, near-infrared and dynamic-mechanical spectroscopies on the curing behaviour, molecular structure and viscoelastic properties of epoxy/anhydride networks

Pellegrino Musto*, Mario Abbate, Giuseppe Ragosta, Gennaro Scarinzi

Institute of Chemistry and Technology of Polymers, National Research Council of Italy, Via Campi Flegrei, 34, Olivetti Building, 80078 Pozzuoli (Naples), Italy

Received 16 June 2006; received in revised form 16 April 2007; accepted 17 April 2007
Available online 4 May 2007

Abstract

The curing characteristics of a TGDDM/HHPA formulation have been investigated by Raman spectroscopy, which allowed us to monitor the evolution of the different reactive species (i.e. epoxy, anhydride and ester groups) participating in the curing process. The curing mechanism and, in particular, the role of side processes, were elucidated. NIR spectroscopy was employed to investigate the post-curing process, in view of the superior sensitivity of this technique for monitoring polar groups. Quantitative methods were developed to measure residual concentration of epoxy groups in the high conversion regimes (≥98%). Dynamic-mechanical measurements were performed to gather information on the molecular structure and viscoelastic properties of the investigated networks. For formulation rich in epoxy resin, clear evidence of an inhomogeneous phase structure was found. A viscoelastic analysis in terms of the WLF approach demonstrated that both the free volume and the thermal expansion coefficient of the networks decrease by enhancing the anhydride/epoxy molar ratio.

Keywords: Raman spectroscopy; NIR spectroscopy; Dynamic-mechanical analysis

1. Introduction

Epoxy resins represent an important class of high-performance materials characterized by properties such as good mechanical and thermal behaviours, high resistance to solvents and corrosive agents, outstanding adhesion to various substrates, low shrinkage upon curing and easy processing under a wide range of conditions [1,2]. These characteristics make them very attractive in a number of demanding, high-technology applications such as, for instance, the encapsulation of microcircuitry in the electronic industry, the development of specialized coatings for highly aggressive environments, the use as matrices for fiber composites in aerospace applications [1–3].

The more reactive and hence more widely employed epoxy hardeners are the amines (aliphatic or aromatic) for which the curing kinetics and mechanism are reasonably well established. Such deep understanding affords a close control of the final molecular structure of the networks by a suitable choice of curing conditions and composition of the reactive mixture [1–3]. In contrast, the information on the curing behaviour of multifunctional epoxies with carboxylic acid anhydrides is rather scarce, even though several of these systems have shown very interesting properties and considerable improvements with respect to their amine-cured counterparts. The epoxy/anhydride systems suffer the limitation of being less reactive, thus requiring higher curing temperatures and larger energy costs. This problem is generally alleviated by using suitable catalysts; Lewis bases such as tertiary amines or imidazoles are the most widely employed.

So far, the more comprehensive studies on the curing behaviour of epoxy/anhydride mixtures have been performed

* Corresponding author.
E-mail address: musto@ictp.cnr.it (P. Musto).

0032-3861/$ - see front matter © 2007 Elsevier Ltd. All rights reserved.
doi:10.1016/j.polymer.2007.04.042

on non-catalysed systems [4–8]. These studies have evidenced that the main esterification reaction is accompanied by concurrent side reactions, among which etherification is favored. Less information is available for catalysed systems, for which several issues remain to be clarified [9,12].

In the present investigation, an epoxy resin system of potential technological interest, namely tetraglycidyl-4,4′-diamino-diphenylmethane (TGDDM) cured with hexahydrophthalic anhydride (HHPA) with 2,4,6 tris-dimethylamino methylphenol (commercial name DMP-30) as an initiator, is investigated in detail. The tetrafunctional TGDDM monomer produces networks with very high cross-link density, which is reflected in T_g values exceeding 270 °C, and exceptional physico-mechanical properties: for this reason TGDDM cured with aromatic diamine hardeners such as 4,4′-diamino diphenylsulfone (DDS) are the preferred resin systems for use as matrices in high-performance fiber composites for aerospace applications. One major deficiency of these formulations is the absorption of relatively large amounts of water in high humidity environments, which brings about a general deterioration of properties [1–3]. The use of an anhydride hardener such as HHPA may result in a number of distinct advantages in comparison to DDS. Particularly relevant is the reduced toxicity of the hardener and the conspicuous decrease in water sorption it imparts to the formulations. Other relevant advantages are a smaller shrinkage and a lower reaction exothermicity [1–3].

One of the aims of the present investigation was to fully develop the potential of a number of molecular characterization tools that are believed to be the most appropriate for these complex networks. Particular attention was paid to choose complementary techniques which could be employed on the same sample, thus avoiding possible changes induced by the preparation procedure and/or the sample thickness or geometry. The second scope was to study the curing behaviour and the resulting viscoelastic properties of the investigated networks. Thus, the kinetics and mechanism of cure were analyzed at a temperature suitable for the system processing (e.g. 140 °C), in order to elucidate the role of side reactions, if any. The selected technique for this purpose was Raman spectroscopy, because it provides a number of key advantages in the present application, with respect to the more conventionally employed FTIR spectroscopy. These advantages are represented by the high quality Raman spectra produced by epoxy systems, the intrinsic sharpness of most bands, which improves significantly the resolution and hence the quantitative analysis, the possibility of monitoring large sample volumes rather than films few μm thick. A further important advantage compared to mid-IR is the possibility to use glass sample holders, not only because of the easier handling and cleaning of the cells, but especially because KBr, the window material for mid-IR, is reported not to be inert but to catalyse the curing of epoxies [7,10]. Raman spectroscopy is very sensitive to polarizable bonds and less so to polar bonds. Therefore, groups such as hydroxyls are not readily detected, particularly when present in low concentration. For this reason the investigation of the post-curing process, which is very relevant for optimizing the curing schedule, especially in the case of non-stoichiometric formulations, has been carried out by means of NIR spectroscopy. This vibrational spectroscopy technique offers the advantages of being insensitive to fluorescence, capable of sampling specimens as thick as those used in the present study, and capable to provide accurate quantitation at trace levels [8]. The second part of the present contribution is devoted to the dynamic-mechanical analysis of the TGDDM/HHPA networks. The aim was to investigate the molecular structure of the network using a probe capable of providing information on segmental motions as well as on more extensive, cooperative transitions. The viscoelastic properties have been also analyzed in detail by using the WLF approach in order to investigate the effect of the stoichiometry, and hence of the cross-link density, on the molecular parameters which characterize the behaviour of these systems as viscoelastic solids.

2. Experimental

2.1. Materials

The epoxy resin was a commercial grade of tetraglycidyl-4,4′-diaminodiphenyl-methane (TGDDM) supplied by Ciba-Geigy (Basel, Switzerland). The hardener was hexahydrophthalic anhydride (HHPA) obtained from Sigma–Aldrich Italy (Milan, Italy). 2,4,6 Tris-dimethylamino methylphenol (DMP-30) supplied by Sigma–Aldrich Italy was used as catalyst. All reagents were used as received with no additional purification.

The chemical structure of the resin components is shown below:

(a) TGDDM – tetraglycidyl-4,4′-diaminodiphenyl-methane

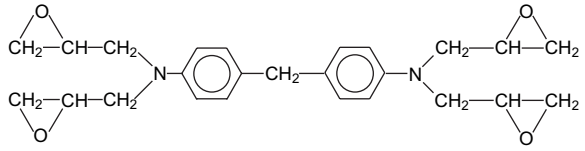

(b) HHPA – hexahydrophthalic anhydride

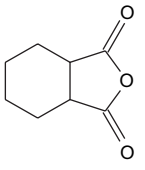

HHPA

In a typical preparation, 100 g of epoxy resin was mixed with 69 g of anhydride at 80 °C in a reaction vessel with provision for mechanical stirring and gas ports. After homogenization, the mixture was degassed under vacuum for 5 min, and 0.51 g of accelerator, DMP-30, was added. After 2 min of mixing, the solution was poured into a glass mold which was immediately transferred in a thermostatic oven and cured at 140 °C for 16 h. The post-cure was continued for 5 h at 200 °C.

The investigated blend compositions are reported in Table 1.

Table 1
Composition, post-curing conversion, water uptake and T_g for the investigated TGDDM/HHPA networks

Composition TGDDM/HHPA (wt/wt)	Molar ratio (mol_{anh}/mol_{epoxy})	α	$A(5245)/L$ (cm^{-2})	H_2O uptake (wt%)	T_g (°C)
100:69	0.45	0.69	114.0	0.49	161
100:80	0.55	0.82	133.0	0.58	183
100:102	0.70	0.92	140.0	0.61	202
100:117	0.80	0.99	162.5	0.71	219
100:144	1.00	1.00	172.4	0.76	220

2.2. Techniques

Raman spectra were collected with a Nexus NIR FT-Raman spectrometer from Nicolet (Madison, WI) equipped with a CaF_2 beam splitter and an indium–gallium arsenide (InGaAs) photoelectric detector. Collection geometry was at 180° backscattered radiation. The excitation source was a diode-pumped Nd-YAG laser ($\lambda = 1064$ nm) operating at a laser power of 750 mW. The spectra were collected in a Raman-shift range between 100 and 3700 cm^{-1} at a resolution of 4 cm^{-1}. Signal averaging over at list 500 data collections was performed to improve the signal-to-noise ratio (SNR). To perform the kinetic measurements, the reactive mixture was filled in several glass vials which were placed in a thermostatic oil bath pre-heated at the desired reaction temperature (140 °C). At prescribed time intervals, the vials were removed, quenched in dry ice and immediately transferred to the Raman sample compartment for the spectrum collection. Raman spectra of post-cured samples were collected on the same specimens used for NIR spectroscopy and dynamic-mechanical analysis, i.e. bars 10.0 mm wide, 50.0 mm long and 1.50 mm thick.

NIR spectra were measured with the same instrument used for Raman spectroscopy, using a Globar source and the alternate sample compartment, equipped with an InGaAs detector. The scanned wavenumber range was 10,000–4000 cm^{-1} and 32 data collections were typically averaged to improve the SNR.

Dynamic-mechanical tests were carried out using a Perkin-Elmer Pyris Diamond DMA apparatus. The geometry of deformation was the single-cantilever bending mode, applying a strain of 1%. The tests were performed in the scanning temperature mode, in the range from −150 to 300 °C at a heating rate of 3 °C/min. At each temperature the frequency was scanned from 0.01 to 20 Hz. The storage modulus (E'), loss modulus (E'') and loss factor (tan δ) were measured as function of temperature at fixed frequency.

3. Results and discussion

3.1. Curing mechanism

In the absence of catalysts the reaction between an epoxy monomer and cyclic anhydrides involves the hydroxyl groups, which act as initiators of the reaction. These groups are present on a fraction of the TGDDM molecules that underwent oligomerization on synthesis. The hydroxyl groups attack the anhydride forming a monoester with a free carboxyl group. This, in turn, reacts with the epoxide ring to yield a diester and a new secondary hydroxyl, which perpetuates the chain process.

In the presence of strong Lewis bases such as tertiary amines, imidazoles or ammonium salts, the mechanism is less clear and still a matter of controversy. The latter proposal [9] assumes the reaction of the tertiary amine with the epoxide ring to form a zwitterion containing an ammonium cation and an alkoxide. The latter rapidly reacts with an anhydride yielding a carboxylate anion. This species represents the active center for the alternating copolymerization reaction. The propagation takes place via the reaction of the carboxylate with an epoxy group, with formation of a new alkoxyde anion. No conclusive evidence has been provided to support a specific termination step and whether the amine initiator remains permanently bounded to chain [9,10]. A schematic representation of the Lewis base catalysed mechanism is depicted below:

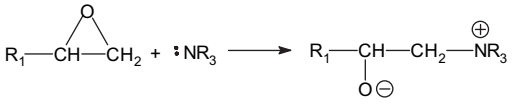
(1)

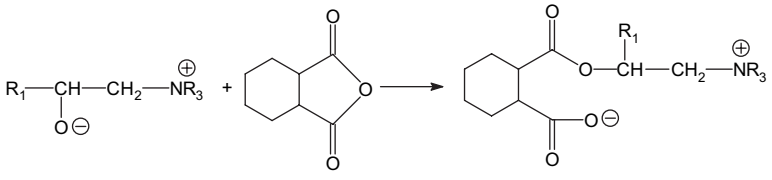
(2)

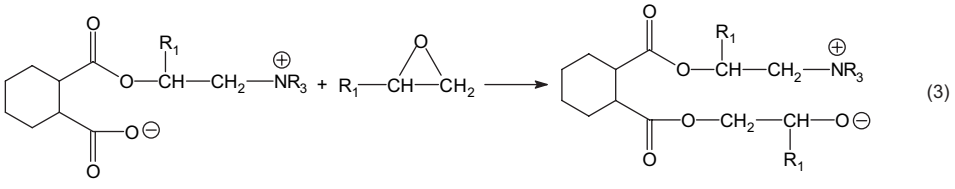
(3)

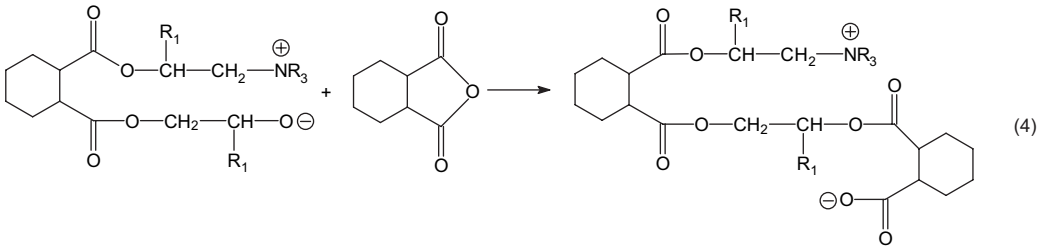

Concurrently with the main mechanism, side reactions can occur, and in particular etherification:

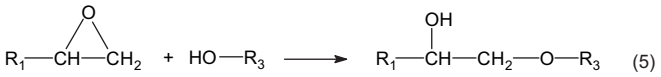

This process plays an important role in non-catalysed systems, while its relevance is lower for the ionic mechanism.

3.2. Raman and NIR spectroscopy

3.2.1. Raman investigation of the curing process

The Raman spectra of TGDDM, HHPA and TGDDM/HHPA mixture prior to curing are reported, respectively, in Fig. 1A–C. The composition of the mixture is 100:69 wt/wt, corresponding to an anhydride/epoxy molar ratio of 0.45. Both the pure components and the reactive mixture display an intense Raman scattering, thus providing good quality, essentially noise-free spectra. Of particular relevance for the present investigation is the intensity and sharpness of most peaks, which afford a conspicuous improvement in terms of resolution in comparison to the allied technique, FTIR spectroscopy. This advantage will be shown to be most relevant for curve fitting analysis. In the ν(CH) region, the TGDDM spectrum displays components at 3071 cm^{-1} (ν Ar-H), 3000 cm^{-1} (ν_{sym} CH_2 epoxy), 2950 cm^{-1} (shoulder), 2919 cm^{-1} (ν_{asym} CH_2) and 2840 cm^{-1} (ν_{sym} CH_2). The di-substituted aromatic rings give rise to several intense peaks at 1614 cm^{-1} (quadrant ring stretching), 1190 cm^{-1} (Ar-H in-plane deformation), 1010 cm^{-1} (Ar-H in-plane deformation), 797 cm^{-1} and 640 cm^{-1}. In particular, the peak at 1614 cm^{-1} is very strong, fully resolved and is invariant with the extent of cure. It is therefore an ideal candidate as an internal standard peak. Contrary to what is observed in the infrared spectrum, the epoxy ring produces two intense Raman features at 1259 cm^{-1} (in-plane deformation of the epoxy ring) and 846 cm^{-1} (CH_2 epoxy deformation) [13,14].

The Raman spectrum of HHPA (Fig. 1B) is considerably simpler that that reported in the literature [9], especially in the ν(CH) region. This is due to the fact that, in the present case, the spectrum has been taken on a molten sample to avoid the additional complication brought about by crystallinity. The symmetric and asymmetric stretching of the carbonyls give rise to two medium intensity peaks at 1854 and 1784 cm^{-1}, respectively. At lower wavenumbers a conspicuous number of sharp and fully resolved peaks are identified, i.e. at 1057, 935, 849, 782, 746, 710, 642, 606, 570, 442, 369, 337, 263, 221 cm^{-1}. Most of the above peaks remain readily detectable in the TGDDM/HHPA mixture (see Fig. 1C) and gradually disappear as the curing reaction proceeds, which demonstrates that the HHPA spectrum is dominated by the deformation modes of the anhydride ring. The only invariant HHPA peak was identified at 1447 cm^{-1} and was attributed to a δ CH_2 mode.

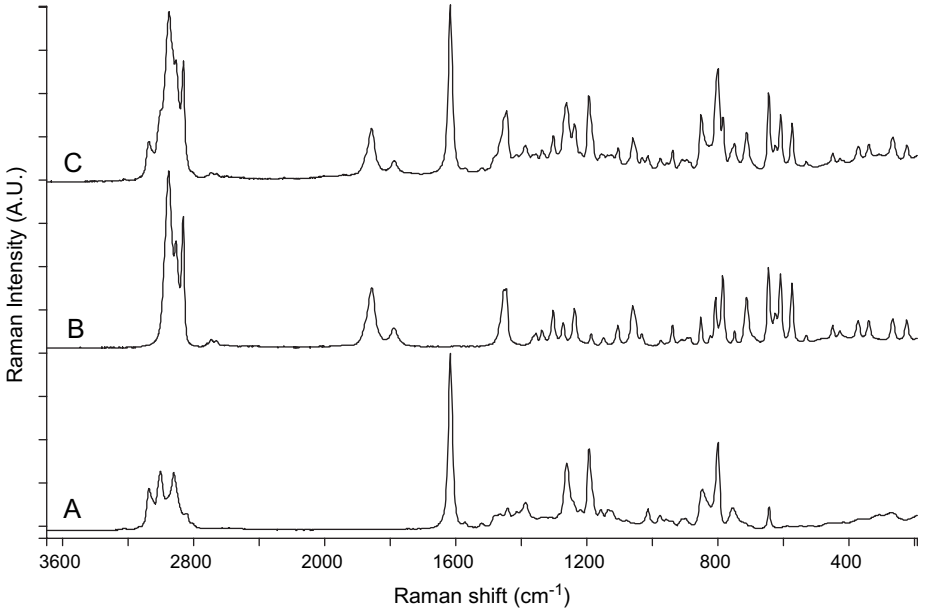

Fig. 1. FT-Raman spectra in the wavenumber range 3700–200 cm^{-1} for (A) TGDDM monomer, (B) HHPA, (C) TGDDM/HHPA mixture 100:69 wt/wt.

Fig. 2 displays the Raman spectra of the reactive mixture taken at different times during the isothermal curing reaction at 140 °C. In particular, Fig. 2A–C refers, respectively, to the wavenumber ranges 2020–1670 cm^{-1}, 1340–1140 cm^{-1} and 1115–1002 cm^{-1}. The esterification involving anhydride and epoxy groups is reflected in the gradual decrease of the anhydride carbonyl peaks and the concurrent development of an ester carbonyl peak at 1737 cm^{-1} (see Fig. 2A). The ester linkage gives rise to a further component at 2963 cm^{-1} (ν_{as} CH_2 adjacent to the ester group).

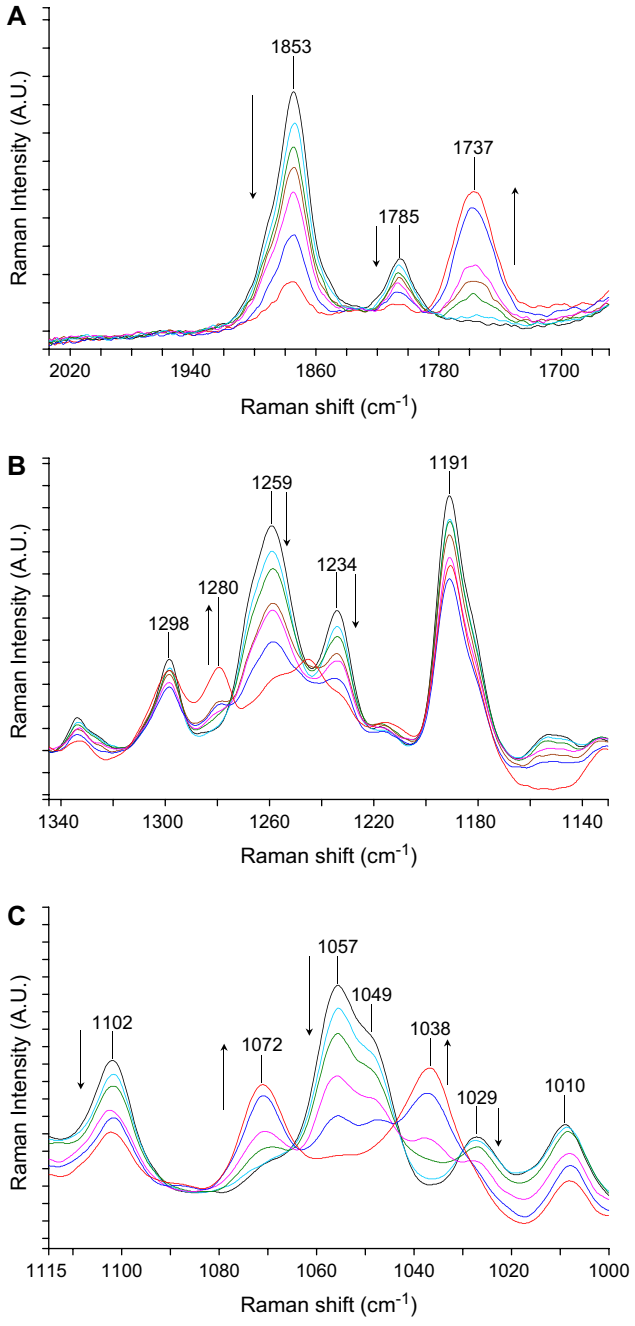

Fig. 2. FT-Raman spectra collected at different times during the isothermal curing reaction of the TGDDM/HHPA mixture at 140 °C. (A) 2020–1680 cm^{-1} interval, (B) 1340–1140 cm^{-1} interval, (C) 1115–1000 cm^{-1} interval.

A quantitative analysis can be approached by assuming the invariance, with extent of cure, of the Raman scattering cross-section, $\partial\sigma_j/\partial\Omega$, which is proportional to the intensity of the jth vibrational mode. In this hypothesis, we may evaluate the relative conversion, α, of a specific functional group from the intensity of one of its characteristic Raman peaks. In fact we may write:

$$\alpha(t) = \frac{C_0 - C_t}{C_0} = 1 - \frac{\left(\frac{I}{I^{1614}}\right)_t}{\left(\frac{I}{I^{1614}}\right)_0} = 1 - \frac{\bar{I}_t}{\bar{I}_0} \tag{1}$$

from which:

$$C_0 - C_t = C_0\left(1 - \frac{\bar{I}_t}{\bar{I}_0}\right) \tag{2}$$

In the above equations I and I^{1614} represent, respectively, the intensity of the analytical and the invariant peaks, and $\bar{I}$ is the normalized intensity. The subscripts 0 and t refer to reaction times zero and t, respectively.

To monitor the anhydride conversion we selected the peaks at 1854 and 570 cm^{-1} for the linearity and reproducibility of the baseline in the latter regions. As for the epoxy group conversion, the 846 cm^{-1} peak is superimposed onto a strong HHPA peak and cannot be reliably resolved. Contrary to what has been reported in the literature [9] even the 1259 cm^{-1} peak is not isolated and the frequency range in which it is located evolves in a quite complex fashion upon curing (see Fig. 2B). However, a curve fitting analysis of the 1340–1140 cm^{-1} wavenumber region gives very reproducible results, owing to the intrinsic sharpness of the components. This is demonstrated in Fig. 3A–C which displays a comparison between the experimental profiles and the curve fitting results for spectra collected at different times during the curing process. It is seen that the simulated profiles are essentially coincident with the experimental ones; furthermore, both the position and the FWHH of the components remain remarkably constant for all the investigated spectra, which confirm the reliability of the analysis.

In Fig. 4A and B are reported, respectively, the normalized intensities of the epoxy peak at 1258 cm^{-1} and the anhydride peak at 1854 cm^{-1}: a sigmoid curve is observed in both cases, with an initial induction period lasting around 5 min. This stage is likely related to the development of a critical concentration of reactive species in the system for the process to reach a steady-state regime.

The latter has a constant reaction rate of 0.060 mol kg^{-1} min^{-1} for the anhydride and 0.085 mol kg^{-1} min^{-1} for the epoxy groups. The steady-state terminates after around 40 min, followed by a sharp drop of the reaction rate, likely due to a liquid-to-solid transition which quenches the cross-link reaction well before the full conversion of the reactants. In fact, the relative conversion of epoxy groups in the plateau region is 0.62, while that of the anhydride hardener is 0.82. Exactly the same kinetic behaviour is found when one considers the ester group formation, as followed by the normalized intensity

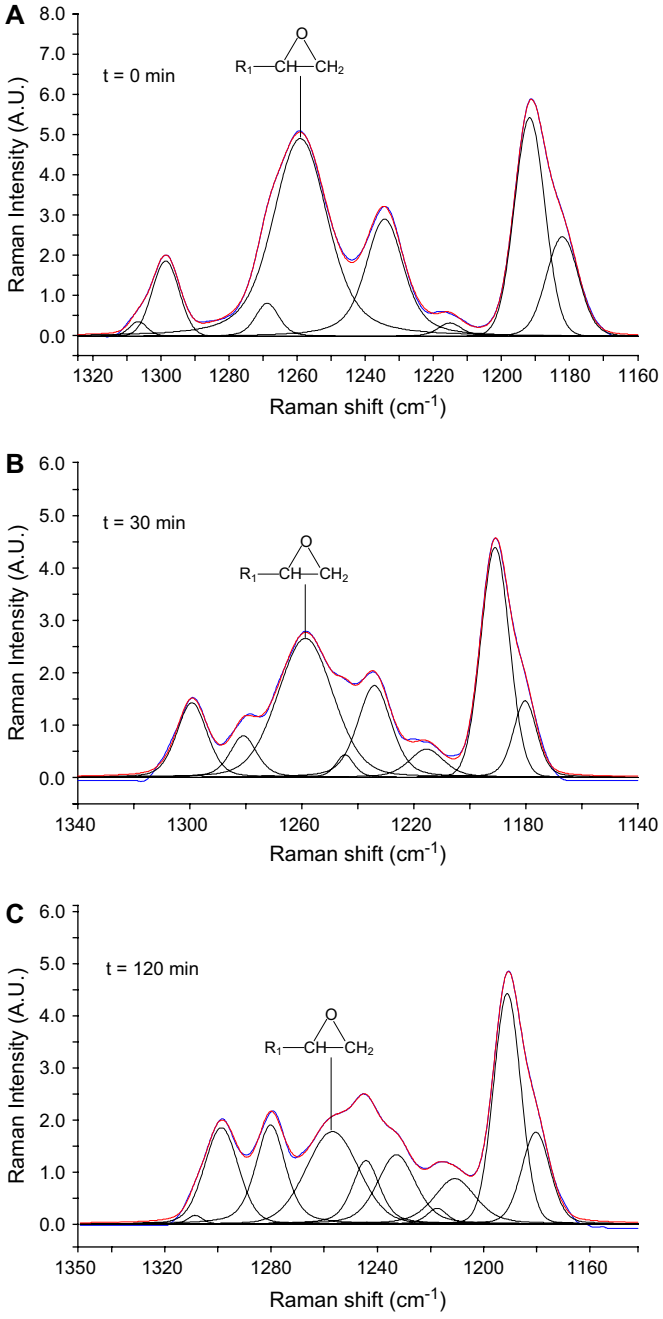

Fig. 3. Curve fitting analysis in the 1320–1140 cm^{-1} interval to isolate the peak relative to the epoxy groups (at 1258 cm^{-1}). Curing times as indicated.

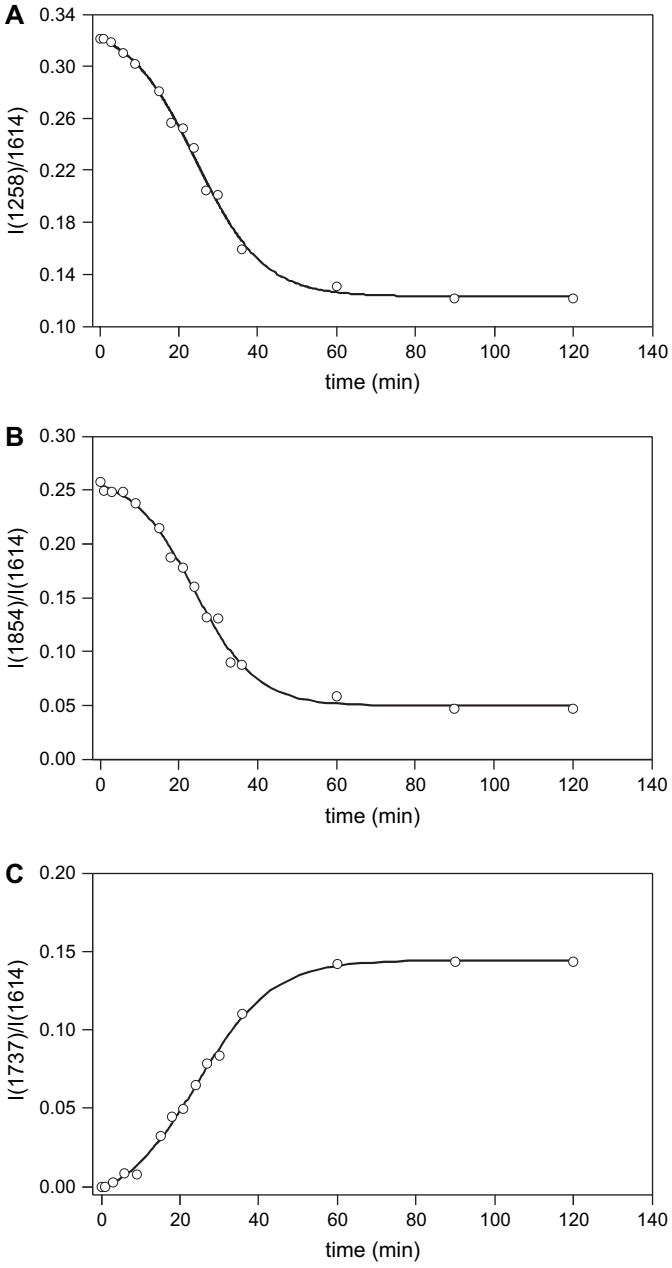

Fig. 4. Normalized intensities of the various characteristic peaks as a function of time for the isothermal curing reaction at 140 °C. (A) Epoxy peak, (B) anhydride peak, (C) ester peak.

of the carbonyl peak at 1737 cm^{-1} (see Fig. 4C). In Fig. 5 is reported the extent of reaction of anhydride and ester groups relative to the final extent of reaction attained at the end of the process (i.e. in the plateau region). This parameter is equal to $(C_0 - C_t)/(C_0 - C_f)$ for the anhydride and C_t/C_f for the ester. The extent of reaction was evaluated from different Raman peaks and the coincidence of the data points onto a single master curve confirms the robustness of the quantitative Raman method.

The occurrence of an induction period in the curing of epoxy resins with anhydride hardeners has been a matter of controversy. Several authors have reported such an effect, i.e. for a stoichiometric mixture of TGDDM and HHPA in the absence of tertiary amine initiators [7] and for a DGEBA/multicomponent anhydride mixture (epoxide/anhydride stoichiometry 1:0.91) [5]. On the other hand, Antoon and Koenig [11] found no evidence of any induction in a kinetic study of a DGEBA/methyl-nadic anhydride mixture cured isothermally between 80 and 100 °C in the presence of a tertiary amine initiator. The spectroscopic data gathered in the present investigation confirm the induction, which is observed in the kinetic profiles of all functional groups (i.e. epoxide, anhydride, ester).

When considering the stationary regime (pseudo zero-order) the different conversion rates of epoxy and anhydride

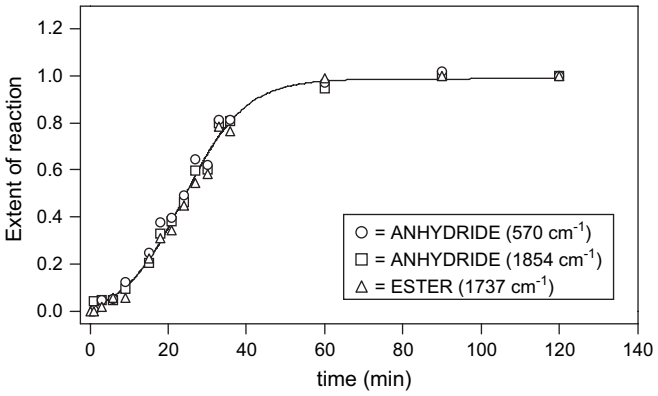

Fig. 5. Relative extent of reaction with respect to the final extent of reaction in the plateau region of anhydride and epoxy groups, as evaluated from different characteristic Raman peaks.

groups point to the occurrence of side processes, concurrently with the principal reaction, i.e., the amine-catalysed esterification. This effect is better appreciated in a conversion–conversion diagram, obtained by plotting the absolute conversion (i.e. $C_0 - C_t$) of epoxy groups versus that of the anhydride functionality. Assuming a purely alternating polyesterification reaction with no side processes, this diagram would produce a linear relationship passing through the origin with a slope equal to one. The present data, reported in Fig. 6, display the expected linear behaviour through the origin, but the slope is higher than expected (1.3 instead of 1.0). Evidently, besides esterification, a further process is active, which consumes epoxy groups; taking into consideration the reactivity of the various functional groups and the reaction temperature, the most probable side process is to be considered the etherification (step 5 of the reaction mechanism reported previously). This process depletes epoxy groups without increasing the net concentration of OH groups, but enhances the cross-link density. In previous studies no evidence of side processes was observed for an non-catalysed TGDDM/anhydride mixture cured at 65 °C [9]. Analogously, Tanaka and Kakiuchi considered different epoxy systems cured at low temperatures and found that etherification was minimal up to the gel point

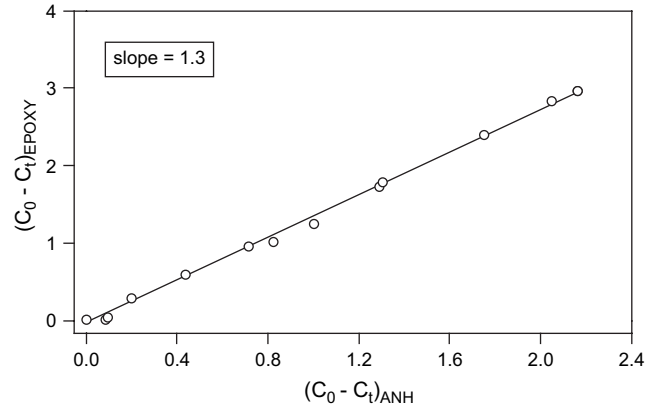

Fig. 6. Absolute conversion of epoxy groups as a function of the absolute conversion of anhydride groups for the isothermal curing at 140 °C.

[15,16]. On the other hand, the reactivity of epoxy with hydroxyl groups in a temperature range from 140 to 250 °C is well established. For instance, for a TGDDM resin cured with diaminodimethylsulfone at 140 °C, after depletion of the highly reactive primary amine groups, the main reaction becomes the etherification which prevails over secondary amine addition [12,17]. Direct spectroscopic evidence of ether group formation cannot be considered conclusive. However, there are three peaks located at 1131, 1072 and 1038 cm^{-1} (see Fig. 2C) which gradually develop as the curing proceeds. They occur in a wavenumber range where ether linkages typically display their C–O–C stretching modes [13,14]; poly(ethylene oxide), for example, displays a doublet at 1141–1125 cm^{-1} and a prominent peak at 1062 cm^{-1}.

In summary, it is concluded that the relevance of etherification in the overall curing mechanism is strongly influenced by factors such as curing temperature and composition of the reactive mixture. In particular this side reaction takes place when curing at 140 °C or above and when the stoichiometry is considerably unbalanced towards the epoxy groups, like in the present case.

3.2.2. Post-curing

The post-curing of the 100:69 TGDDM/HHPA mixture, carried out at 200 °C for increasing time periods, brings about well detectable spectral changes, as well as structural modifications which will be discussed in detail in the foregoing paragraphs. In Fig. 7 are reported the FT-Raman spectra in the 3600–400 cm^{-1} of the TGDDM/HHP mixture (composition 100:69 wt/wt), post-cured at 200 °C for 5 h (trace A), 11 h (trace B) and 21 h (trace C). As the post-curing time rises, the initially flat baseline becomes increasingly steep. This indicates that the sample becomes increasingly fluorescent, as a consequence of the formation of conjugated structures within the polymer network. These structures, which involve carbon–carbon unsaturations and carbonyl groups, are likely the result of thermo-oxidative degradation processes taking place at 200 °C [18,19]. However, these reactions are generally diffusion limited and are confined to a narrow surface layer of the sample. They strongly affect the scattering process since the radiation has to cross the surface, but can be considered negligible if one considers the overall molecular structure of a sample 1.50 mm thick. Besides fluorescence, the Raman spectra of the samples post-cured for various times are otherwise very similar to each other. The only detectable difference is highlighted in the inset of Fig. 7 and is related to the gradual decrease of the residual epoxy peak at 1259 cm^{-1}.

The post-curing reactions have been further investigated by FT-NIR spectroscopy, owing to the superior sensitivity of this technique to hydrogen-containing groups such as O–H and C–H. In Fig. 8 are reported the NIR spectra recorded in the wavenumber range 9200–4500 cm^{-1} of a TGDDM/HHPA sample (composition 100:69 wt/wt) cured at 200 °C for 5 h (trace A) and 30 h (trace B). The insets highlight the evolution of the spectra with post-curing at times indicated. Being the NIR spectrum unaffected by fluorescence, all spectra display the same optimum quality. The two peaks characteristic of

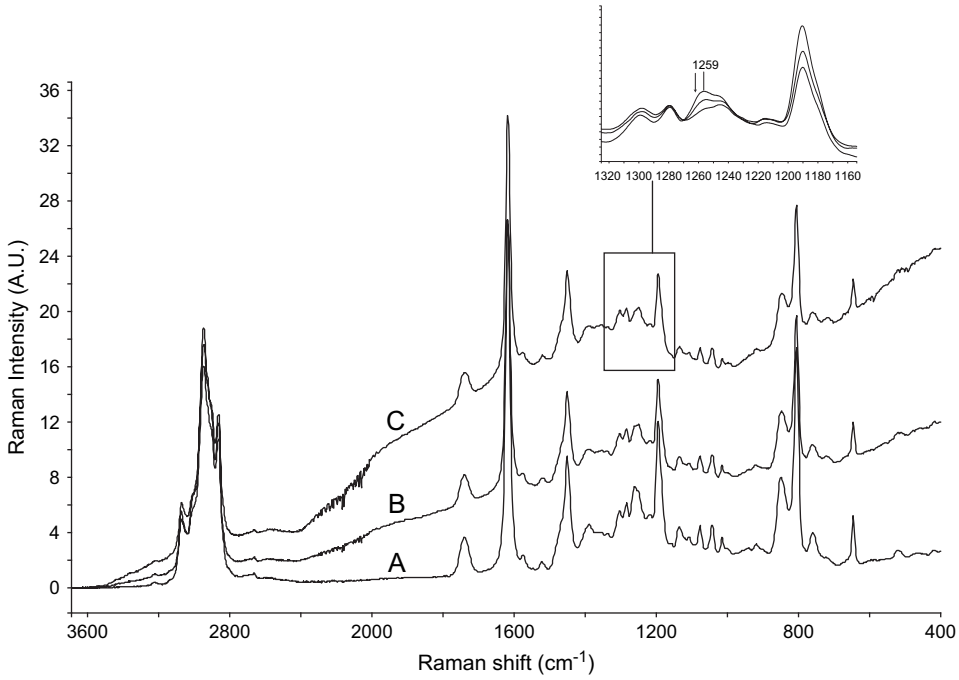

Fig. 7. FT-Raman spectra in the wavenumber range 3600–400 cm^{-1} for the TGDDM/HHPA mixture having a composition 100:69 wt/wt. Trace A: sample post-cured at 200 °C for 5 h. Trace B: sample post-cured at 200 °C for 11 h. Trace C: sample post-cured at 200 °C for 21 h. The inset highlights the region where the characteristic peak of residual epoxy group is located.

the oxyrane ring at 4520 cm^{-1} and 6055 cm^{-1} (overtone of the terminal CH_2 stretching) decrease gradually up to total depletion after 30 h. Concurrently, a broad band, initially centered at 6990 cm^{-1}, associated with the overtones of the O–H stretching modes, is found to increase. It is tempting to directly associate the two processes, i.e. to assume that the hydroxyl groups are the products of an epoxy group reaction. However, in the system at hand, no functionality is present which could produce O–H groups by reacting with an epoxy ring, except, possibly, trace amounts of secondary amines present as impurities on TGDDM, and due to incomplete reaction of diaminodiphenyl-methane with epichlorohydrin during the monomer synthesis. Although these species have been actually detected [20], their concentration is to be considered too low to account for the total increase of hydroxyl groups in the system. In fact, the absorbance

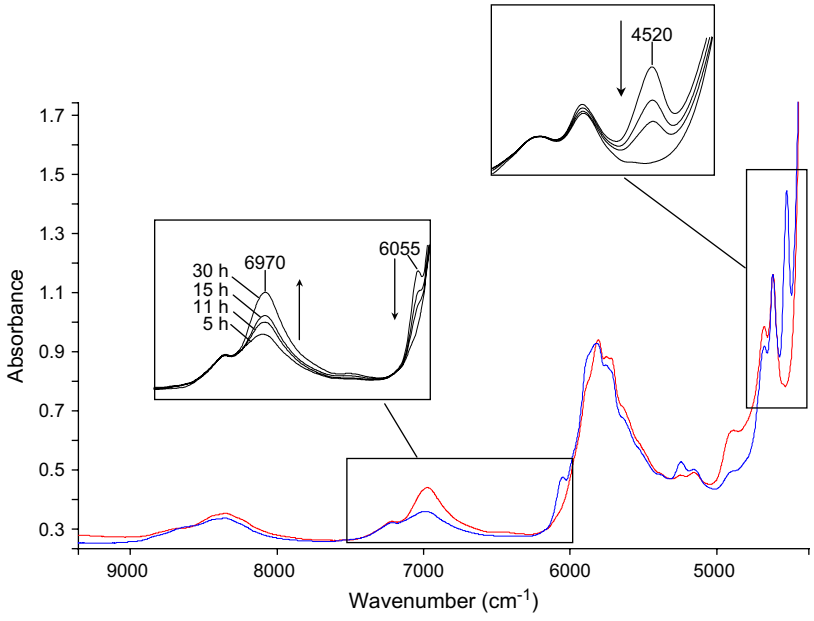

Fig. 8. FT-NIR spectra in the wavenumber 9500–4000 cm^{-1} for the TGDDM/HHPA mixture with composition 100:69 wt/wt post-cured at 200 °C for 5 h (blue trace) and 30 h (red trace). The insets highlight the relevant wavenumber ranges comparing the spectra post-cured for various times as indicated. (For interpretation of the references to colour in this figure legend, the reader is referred to the web version of this article.)

area of the ν_{O-H} band increases by as much as 56% after 30 h post-curing with respect to the value after 5 h post-curing, which, assuming an average absorptivity value for the whole band, would correspond to the same increase in concentration.

It is not straightforward to account for the spectroscopic observations in the NIR interval. Our hypothesis is that, while the decrease of the epoxy peaks is mainly due to etherification, the enhancement of the ν_{O-H} band is to be related to several concurrent factors. The reaction of epoxy groups with amine impurities may play a limited role. The main effect could be associated with a rearrangement of the H-bonding interactions between self-associated O–H groups within the network. Thus, more interactions can be formed upon post-curing as a consequence of the molecular mobility in the proximity of the T_g and because of the increase in cross-link density of the network caused by the etherification reactions. It is known that a H-bonding interaction causes an increase of the molar absorptivity of the ν_{O-H} band, albeit the effect is smaller in the NIR range than in the mid-IR [21,22]. Therefore, the observed enhancement of the ν_{O-H} signal may arise from an enhancement of the absolute integrated intensity, rather than to a concentration increase of the absorbing species, i.e. a physical effect rather than a chemical one.

Further insight in the mechanism of the post-curing process is gained by considering samples with different anhydride/epoxy molar ratio, R, post-cured for 5 h at 200 °C. Their NIR spectra (normalized for the sample thickness) are compared in Fig. 9, in the wavenumber range 6300–4400 cm^{-1}. As expected, the residual amount of epoxy groups decreases gradually with R, as evidenced by the oxyrane peaks at 6055 and 4520 cm^{-1}. A method was developed for a quantitative estimation of the residual epoxy group concentration from the spectra of Fig. 9. The samples were brought to full conversion by heat treatment at 200 °C for additional 20 h and their spectra were subtracted from those of the starting samples. Since the spectral changes are essentially limited to the epoxy peaks, this subtraction procedure serves to improve their resolution, as demonstrated in the inset of Fig. 9. The quantitative analysis was performed by considering the height of the 6055 cm^{-1} peak, for which the molar absorptivity value was accurately measured beforehand (0.0270 mol mm kg^{-1}). The results of the quantitative analysis are collectively reported in Table 1. It is found that, for the sample with $R = 0.45$ the epoxy conversion, α, after post-curing is 0.69, consistent with the value of 0.60 obtained by Raman spectroscopy after the isothermal curing at 140 °C. The conversion increases with R and is complete only at $R = 1$. At $R = 0.80$ a residual epoxy concentration of 1.0% with respect to the initial value, still produces well detectable signals, thus confirming the superior sensitivity and accuracy of NIR spectroscopy in the high conversion regimes.

A band located at 5242 cm^{-1} (see Fig. 9) is due to the $\nu_s^{01}(OH) + \delta^{01}(OH)$ vibrational transition of absorbed water. From its integrated intensity it is possible to quantitatively evaluate the amount of sorbed water at equilibrium under normal atmospheric conditions (25 °C, 50% RH). A calibration curve constructed by plotting the band area as a function of sorbed water evaluated gravimetrically was used to convert the values of integrated absorbance (normalized for sample thickness) into weight percent of sorbed water. The results are reported in the 5th column of Table 1. A slight enhancement of the water content is noticed as the R value increases, which likely reflects the increased concentration of ester carbonyls in the networks at higher R values. These groups have been demonstrated to form H-bonding interactions with water molecules acting as proton acceptors, thus enhancing the interactive character of the network [23,24]. In any case, the equilibrium water sorption goes from 0.49% to 0.76% and is considerably lower than that for a TGDDM/DDS resin, which in the same conditions absorbs 4.0% of water [25]. This confirms the superior properties of the TGDDM/HHPA system in connection with environmental inertness.

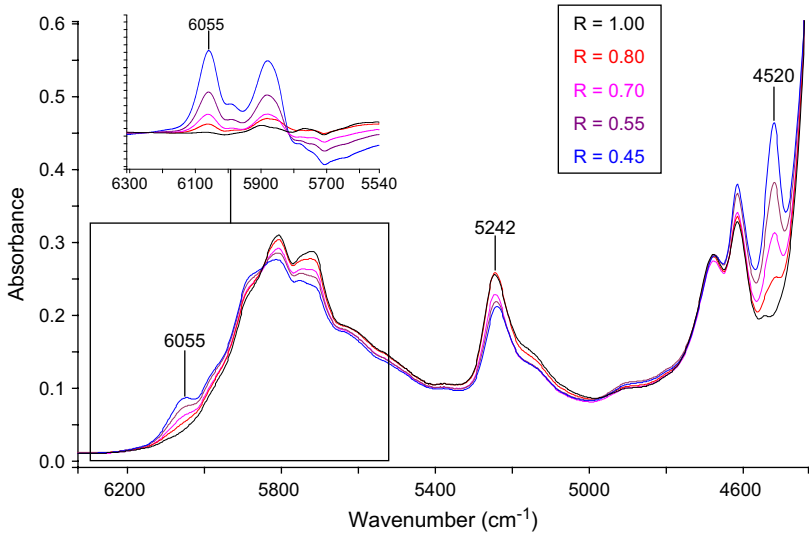

Fig. 9. FT-NIR spectra in the wavenumber range 6300–4440 cm^{-1} for TGDDM/HHPA mixtures with different compositions, post-cured at 200 °C for 5 h. The anhydride/epoxy ratio, R, is indicated in the box. The inset displays the subtraction spectra used for quantitative analysis (see text for details).

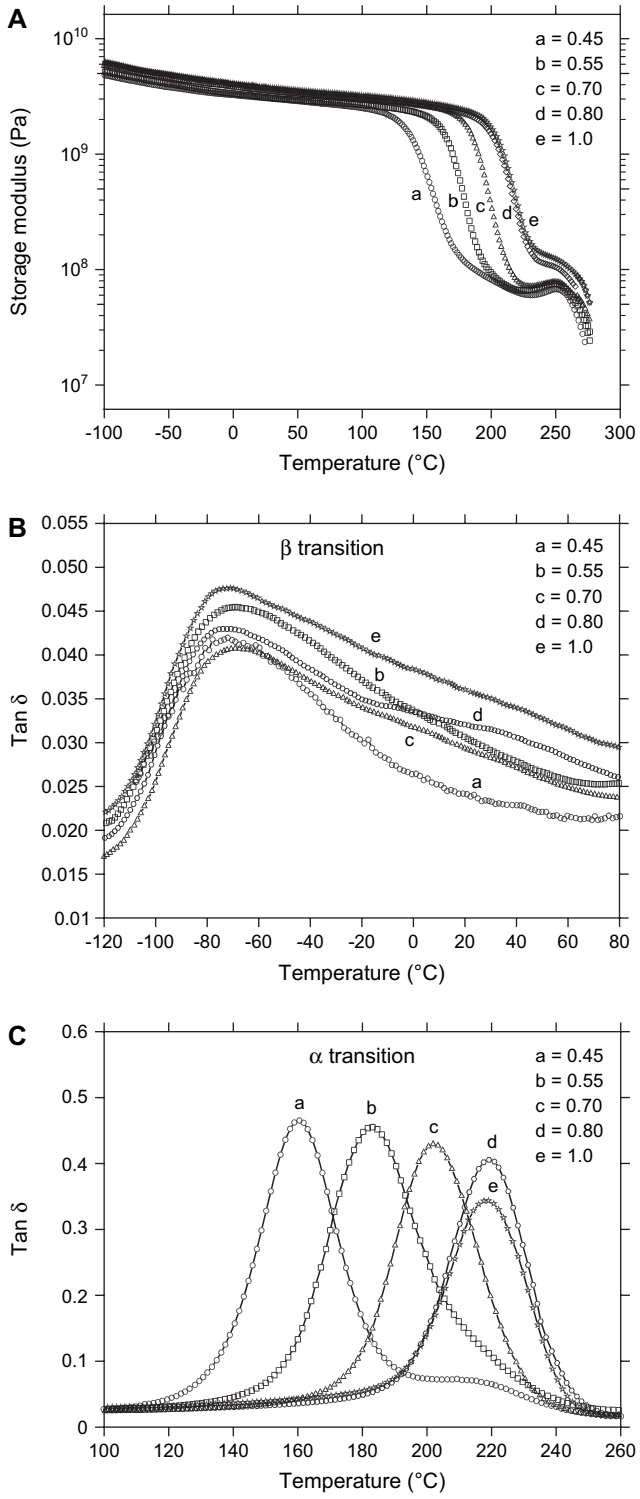

Fig. 10. (A) Storage modulus (E') as a function of temperature for the TGDDM/HHPA mixtures of different composition. Molar ratio as indicated. (B) Loss factor (tan δ) as a function of temperature in the range −120 to 180 °C for the TGDDM/HHPA mixtures at different composition. Molar ratios as indicated. (C) Loss factor (tan δ) as a function of temperature in the range −100 to 260 °C for the TGDDM/HHPA mixtures at different composition. Molar ratio as indicated.

3.3. Dynamic-mechanical properties

Dynamic-mechanical spectra in terms of storage modulus (E') and tan δ at 1 Hz for TGDDM/HHPA mixtures with different stoichiometric ratios are displayed in Fig. 10A–C. All systems show two distinct relaxation peaks: the broad band at low temperature (Fig. 10B) is usually denoted as the β transition and is associated with isolated motions of small units of the network. In the case of epoxy/anhydride networks, the β transition has been attributed to the anhydride moiety incorporated into the network through diester linkages [26,27]. The elastic modulus, E' (Fig. 10A), decreases slightly through the β transition. The high temperature relaxation (Fig. 10C) is an α transition process and corresponds to the T_g. In this glass–rubber transition region, E' shows a sharp drop of almost two orders of magnitude, before leveling off in the rubbery region.

It is generally reported [28–30] that peak position, height and width of both α and β transitions depend on the cross-link density of the epoxy network. In Table 2 are summarized the main characteristics of the β transition, including the apparent activation energy, which was evaluated by a multi-frequency analysis and by considering an Arrhenius dependence of the type:

$$f = A \cdot \exp(-E_{a,\beta}/RT) \tag{3}$$

where f is the frequency, A is the pre-exponential factor, R is the gas constant, T is the relaxation peak temperature and $E_{a,\beta}$ is the activation energy.

The values of $E_{a,\beta}$ were evaluated from the slopes of the curves obtained by plotting the logarithm of frequency versus the reciprocal of the relaxation peak temperatures.

The data of Table 2 show a negligible effect of the stoichiometric ratio on the β parameters, suggesting that this transition is independent of the molecular mobility and concentration of the diester segments present in the epoxy network. This is supported by the finding that the activation energy is essentially constant for all formulations. It is also found (see Table 2) that the experimental $E_{a,\beta}$ values are coincident with those derived by the theoretical approach proposed by Starkweather [31,32], assuming an activation entropy, ΔS, for the relaxation process close to zero. This demonstrates that the molecular motions involved in the β process are essentially non-cooperative, in agreement with earlier literature data [30,33].

In contrast, the composition of the TGDDM/HHPA mixture has a large effect on the α transition. As clearly evidenced by

Table 2
Characteristics of the β transition

Molar ratio (mol_{anh}/mol_{epoxy})	Height of the β transition	T_β (°C)	$E_{a,\beta}$ [a] (kJ/mol)	E_a [b] (kJ/mol)
0.45	0.021	−73.2	48.5	46.8
0.55	0.023	−69.5	48.1	47.7
0.70	0.020	−69.2	50.5	47.7
0.80	0.023	−72.3	49.7	47.1
1.0	0.022	−71.0	47.8	47.3

[a] From the multi-frequency analysis.
[b] From the Starkweather method.

Fig. 10A and C, the E' drop and the peak temperature of the α relaxation increase with increasing the stoichiometric ratio, R, while an opposite trend is observed for the height of the α peak. Both these features confirm that the cross-link density of the networks increases with an increasing R.

The rubber elasticity theory [34], along with the experimental storage modulus in the rubbery region were used to estimate the cross-link density of the investigated networks. The equation used was:

$$M_c = \frac{3\rho RT}{E_r} \tag{4}$$

where M_c is the average molecular weight between two cross-link points, ρ is the density of the network at the absolute temperature T, R is the gas constant, and E_r is the rubbery modulus, defined in this study as the value of E' at 40 °C above its α relaxation peak.

The dependence of M_c and T_g on R is shown in Fig. 11A, while Fig. 11B displays the M_c and T_g values as a function of the epoxy group conversion after post-curing, as evaluated spectroscopically (see Table 1). M_c and T_g exhibit an opposite trend, i.e. M_c decreases and T_g increases as the anhydride/epoxy ratio increases. This behaviour can be related to the degree of polymerization reached for each formulation at the end of the curing and post-curing processes. For compositions near to stoichiometry ($R = 0.8$ and 1.0) whereby the conversion of reagents is almost complete, densely cross-linked networks with enhanced T_g are formed. On the contrary, for epoxy-rich formulations the low amount of anhydride units with respect to the epoxy groups, prevents the completion of the curing reaction developing networks with lower cross-linking density and lower T_gs. If we consider, in place of the initial composition, a more meaningful parameter such as the epoxy group conversion, α, which is quantitatively related to the cross-linking density, the T_g exhibits a linear dependence (see Fig. 11B). On the other hand, M_c remains almost constant up to conversion values close to 0.85, thereafter displaying a sharp decrease. Thus, the M_c parameter is generally less sensitive to the reactant conversion than T_g; only in the very high conversion regimes, small variations of α induce conspicuous changes in M_c. This demonstrates how sensitive the molecular structure of the network is to the post-curing process, and how important is to optimize and control this thermal treatment. In this light, the importance of a technique able to quantify trace amounts of unreacted groups, like NIR spectroscopy, is further stressed.

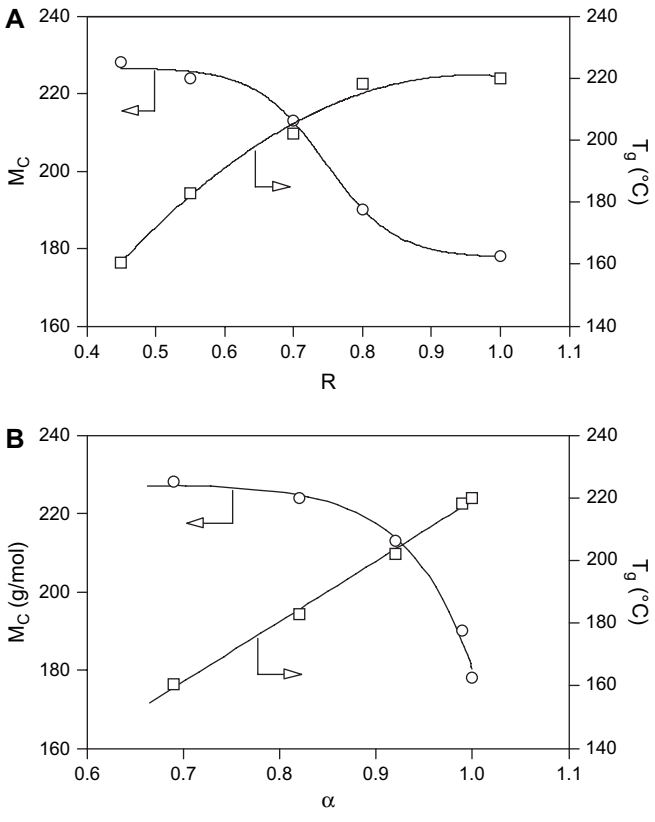

Fig. 11. (A) M_c and T_g as a function of the epoxy/anhydride molar ratio (R). (B) T_g and M_c as function of the final conversion of epoxy groups (α).

For the formulations with low anhydride content (R between 0.45 and 0.70) the spectroscopic measurements previously discussed demonstrated that additional heating treatments, after the standard curing protocol, produced new cross-linking reactions in which the unreacted epoxy groups were involved. The effect of these heating treatments on the characteristics of the networks formed is shown in Fig. 12A and B for the resin with the lowest anhydride/epoxy ratio ($R = 0.45$). These plots compare, in the temperature range between 100 and 260 °C, the E' and tan δ curves of samples cured with the standard cure schedule (curve a) and those isothermally treated at 200 °C for additional 6, 10, 20 and 30 h, respectively (curves b–e). As can be seen, this further post-curing process causes a marked shift of the T_g towards higher temperatures and an increase of E' in both glassy and rubbery regions. Moreover, the slight shoulder around 215 °C, present in the tan δ curve of the reference sample (curve a of Fig. 12B), increases markedly with post-curing time (curves b and c). At post-curing times of 25 h or higher (curves d and e) the shoulder disappears, and narrower tan δ peaks, with maxima at around 210 °C, are observed.

The occurrence of a second relaxation peak at higher temperature besides the main α transition, in the sample post-cured for 5 h, is indicative of the inhomogeneity of the network's molecular structure. The heterogeneity of the system is induced by the post-curing treatment, i.e. by the chemical reactions occurring in this regime, which, according to the spectroscopic evidence, are mainly represented by the etherification of the residual epoxy groups. It can be devised that these processes induce a local densification of the material caused by an increase of cross-link density. Denser nodules, uniformly distributed within a matrix at lower cross-link density, are thus formed, which are responsible for the high temperature relaxation. As the post-curing time increases, the initially small nodules tend to grow in dimensions as a consequence of further etherification with neighboring chains, thus involving larger and larger regions of the material, at

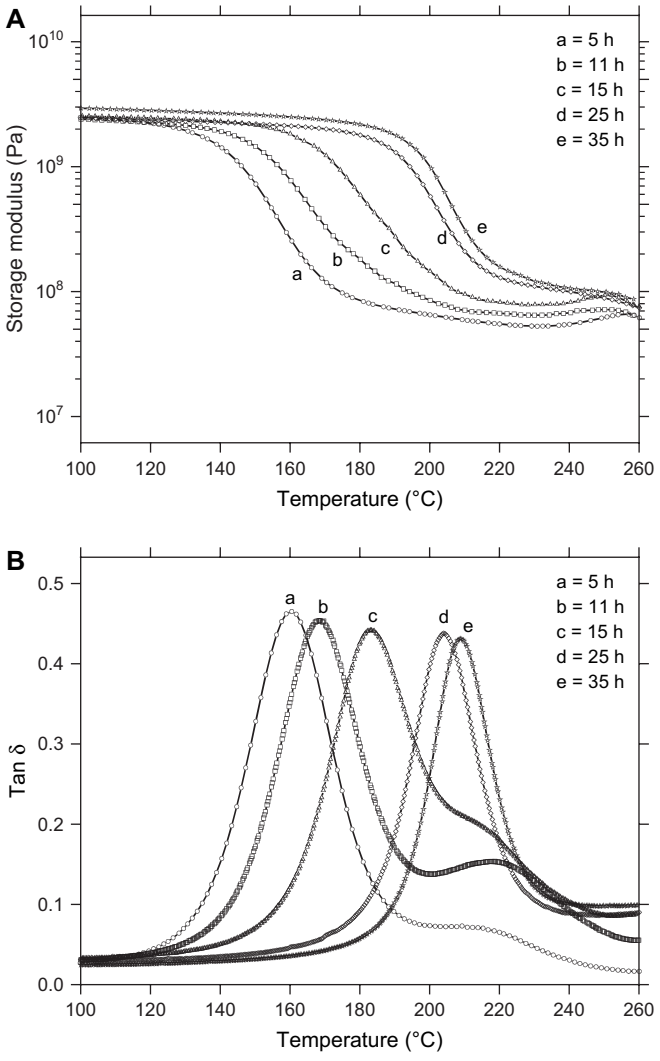

Fig. 12. (A) Storage modulus (E') as a function of temperature in the range 100–260 °C, for the TGDDM/HHPA formulation with $R = 0.45$. Measurements taken after post-curing at 200 °C for various times, as indicated. (B) Loss factor (tan δ) as a function of temperature in the range 100–260 °C, for the TGDDM/HHPA formulation with $R = 0.45$. Measurements taken after post-curing at 200 °C for various times, as indicated.

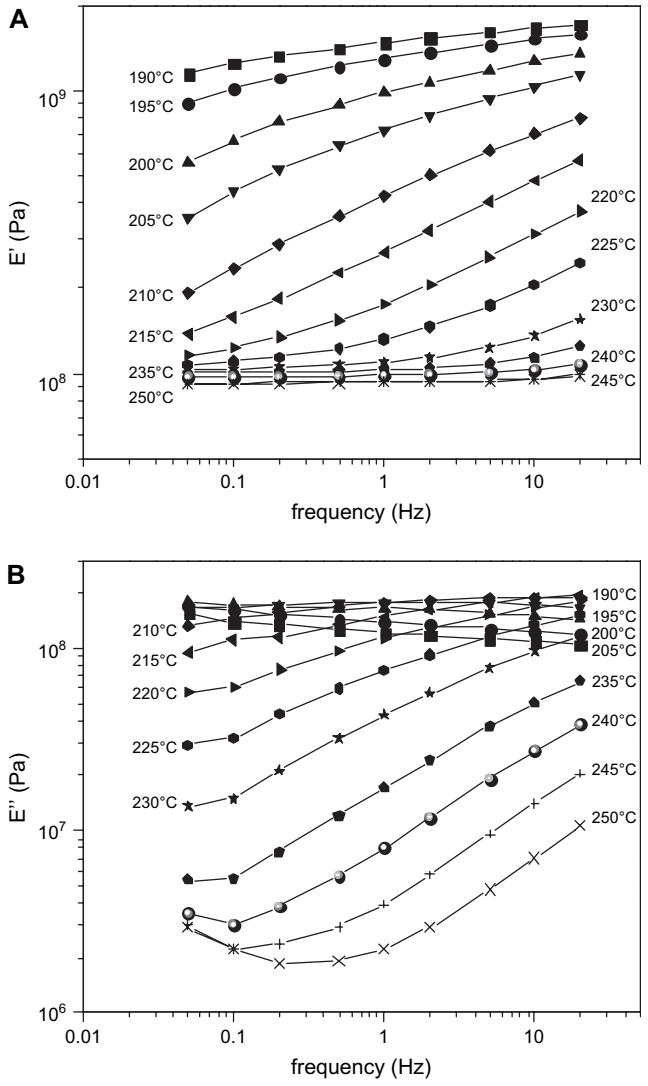

Fig. 13. (A) Storage modulus (E') isotherms as a function of frequency in the range 0.01–50 Hz, for the TGDDM/HHPA mixture with $R = 1$. (B) Loss modulus (E'') isotherms as a function of frequency in the range 0.01–50 Hz, for the TGDDM/HHPA mixture with $R = 1$.

the expenses of the low cross-link density matrix. This is reflected in the increasing contribution of the high temperature relaxation with respect to the one at lower temperature, characteristic of the matrix.

It is to be noted that the position of the principal relaxation also moves upward upon post-curing and the shift increases with post-curing time. This effect is not to be ascribed to the enhancement of the cross-link density of the matrix itself, but rather to the reinforcing effect of the nodules which are tightly interconnected with the matrix through covalent bonds. As the nodules grow up and become denser, the reinforcing effect is enhanced and the T_g of the matrix increases. Beyond a critical post-curing time ($\geq$20 h) the nodules have grown enough to involve the entire network, thus starting to interact with each other. In these conditions the two-phase system tends to coalesce again, leading to the occurrence of a homogeneous molecular structure whose characteristics, in terms of T_g and M_c, closely resemble those of formulation with higher R ratios.

3.4. Viscoelastic analysis of the epoxy networks in the glass transition region

The dynamic-mechanical data, obtained by multi-frequency experiments as a function of temperature, were used to evaluate the viscoelastic parameters of the various networks in the glass transition region. In Fig. 13A and B are shown, for the formulation with an epoxy/anhydride ratio of 1, the variation of E' and E'' as a function of frequency in the temperature range from T_g −30 °C to T_g +30 °C. Similar diagrams were obtained for the other TGDDM/HHPA mixtures. According to the time–temperature superposition principle [35], the isothermal curves of Fig. 13A and B can be shifted on the frequency scale to produce master curves over an enhanced

frequency range at a reference temperature T_0 [36]. In principle, a vertical shift $\rho T/\rho_0 T_0$ should also be applied to account for the variation in polymer density (ρ) between T and T_0. In our case this correction is negligible owing to the narrow temperature range under consideration. Thus, master curves were built up without making any vertical shift. In Fig. 14 are shown the master curves for both E' and E'', obtained from Fig. 13A and B, in which the T_g at 1 Hz was taken as the reference temperature.

In the glass transition region, the temperature dependence of the shift factor, a_T, obeys the well-known Williams–Landel–Ferry (WLF) equation [35,36]:

$$\log a_T = -\frac{C_1^g(T-T_0)}{C_2^g + T - T_0} \tag{5}$$

where C_1^g and C_2^g are the values of the viscoelastic coefficients at T_g. According to Eq. (5), these parameters can be derived by plotting $T-T_g/\log a_T$ against $(T-T_g)$. As shown in Fig. 15, the values of a_T, deduced from the E' and E'' curves, produce an unique straight line, indicating that the viscoelastic behaviour of the material follows correctly the time–temperature superposition principle. The coefficients C_1^g and C_2^g are given, respectively, by the reciprocal of the slope and the intercept of the straight line of Fig. 15. The WLF parameters evaluated with this procedure for the investigated TGDDM/HHPA networks are summarized in Table 3.

Both C_1^g and C_2^g decrease as the stoichiometric ratio, i.e., the cross-linking density, is reduced. However, the variation from one system to the other is rather small.

The C_1^g and C_2^g parameters bear a molecular level information, in that they are related to the network topology through the following equations:

$$C_1^g = \frac{B}{2.3 f_g} \text{ and } C_2^g = \frac{f_g}{\alpha_f} \tag{6}$$

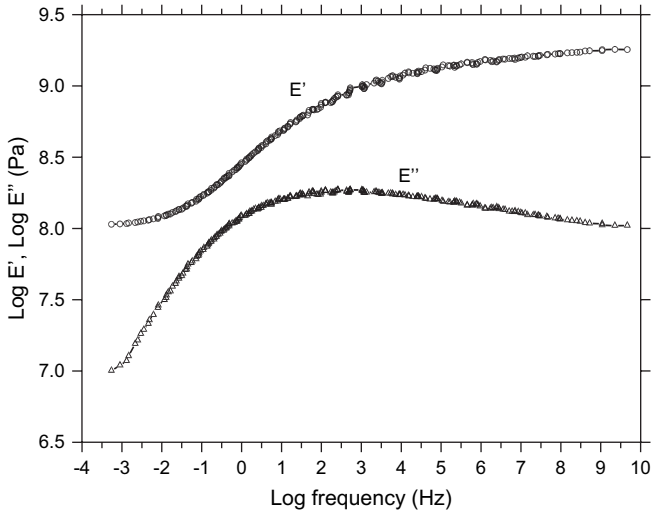

Fig. 14. Master curves for the storage modulus (E') and loss modulus (E'') relative to the TGDDM/HHPA mixture with $R = 1$.

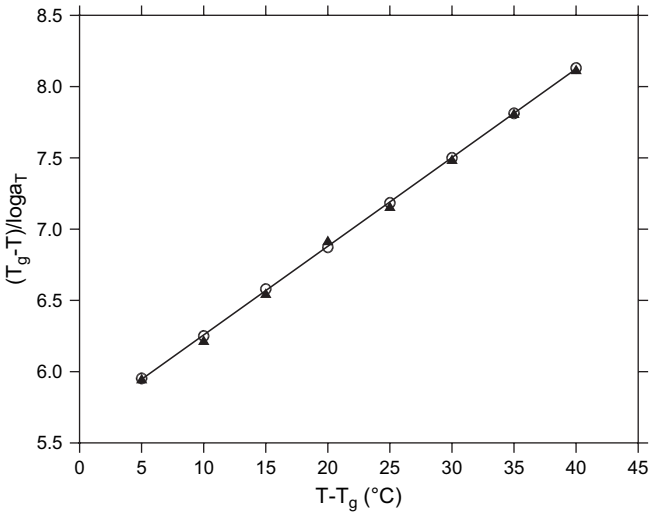

Fig. 15. Evaluation of the viscoelastic parameters C_1^f and C_2^f from the shift factors of the master curves E' (□) and E'' (■) for the TGDDM/HHPA mixture with $R = 1$.

where f_g is the free volume fraction at T_g, α_f is the thermal expansion coefficient of the free volume and B is an empirical constant generally considered to be close to unity [36].

Values of f_g/B and α_f/B computed from the above equations are reported in Table 3. It can be observed that both f_g/B and α_f/B decrease with increasing the stoichiometric ratio, consistently with the fact that, enhancing the cross-link density of the network reduces the free volume and the tendency of the system to undergo thermal expansion. Both these parameters are relevant with respect to the material's performances. In fact, high residual free volume considerably enhances the rate of penetration of low molecular weight compounds, such as water, methanol, organic solvents, etc., thus promoting undesired plasticization effects and/or damages to the interface regions in the case of composites. Furthermore, the dimensional stability is a stringent requirement both for processing purposes and for optimizing service performances in applications such as microcircuitry encapsulation or high-performance adhesive coatings. The present results, therefore, point to a complex interplay between mixture composition, curing kinetics and mechanism, processing conditions and molecular structure of the resulting network. The final molecular structure, in turn, controls the system performances through the excess free volume and the coefficient of thermal expansion. Therefore, there is a need to deepen our understanding of the structure–properties correlations, in order to design and optimize materials with tailor-made properties.

Table 3
Viscoelastic characteristics of the epoxy networks

Molar ratio (mol_{anh}/mol_{epoxy})	C_1^g	C_2^g (°C)	$C_1^g C_2^g$ (°C)	$f_g/B \times 10^2$	$\alpha_g/B \times 10^3$
0.45	12.3	87.7	1078.7	3.53	0.41
0.55	13.1	88.1	1154.1	3.31	0.37
0.70	13.6	88.8	1207.7	3.19	0.36
0.80	14.4	89.3	1285.9	3.02	0.34
1.0	16.1	90.1	1450.6	2.70	0.30

4. Concluding remarks

In the present contribution the curing behaviour of a TGDDM/HHPA formulation has been investigated by Raman spectroscopy. The quantitative accuracy and superior resolution of this spectroscopic technique allowed us to concurrently monitor the kinetic profiles of all reactive groups participating in the process, i.e. epoxy, anhydride and ester groups. Information has been gained about the mechanism and the side reactions (etherification) taking place at a curing temperature suitable for actual processing. The post-curing process, very relevant in view of optimizing processing conditions, especially for non-stoichiometric formulations, has been investigated by NIR spectroscopy. The superior sensitivity of this technique for monitoring polar groups has been demonstrated, and suitable quantitative methods has been developed to quantify the residual concentration of epoxy groups in the high conversion regimes ($\geq$98%). A dynamic-mechanical analysis has been used to gain an insight into the molecular structure and viscoelastic properties of epoxy networks differing in terms of composition and/or curing conditions. Clear evidence has been found in an inhomogeneous phase structure when the molar ratio between the resin components is strongly unbalanced towards the epoxy monomer. This two-phase structure was attributed to the occurrence of nodules of higher crosslinking density uniformly dispersed within a matrix at a lower level of cure. However, further heat treatment for prolonged time periods tends to homogenize the structure. No such effect has been detected when the anhydride/epoxy molar ratio tends to unity. Finally, a viscoelastic analysis in terms of the WLF approach has allowed us to evaluate the characteristic parameters C_1^g (related to the free volume) and C_2^g (associated with the thermal expansion coefficient) for the investigated networks. It has been shown that both the above parameters decrease by enhancing the anhydride/epoxy molar ratio.

References

[1] May CA, editor. Epoxy resins, chemistry and technology. 2nd ed. New York: Marcel Dekker Inc.; 1988.
[2] Lee H, Neville K. Handbook of epoxy resins. New York: McGraw-Hill; 1990.
[3] Ellis B, editor. Chemistry and technology of epoxy resins. Glasgow: Blackie Academic and Professional; 1993.
[4] Stevens GC. J Appl Polym Sci 1981;26:4259.
[5] Stevens GC. J Appl Polym Sci 1981;26:4279.
[6] Woo EM, Seferis JC. J Appl Polym Sci 1990;40:1237.
[7] Corcuera MA, Mondragon I, Riccardi CC, Williams RJ. J Appl Polym Sci 1997;64:157.
[8] Siesler HW, Ozaki Y, Kawata S, Heise HM. Near-infrared spectroscopy. Weinheim, Germany: Wiley-VCH; 2002.
[9] Rocks J, Rintoul F, Vohwinkel F, George G. Polymer 2004;45:6799.
[10] St. John NA, George GA. Polymer 1987;33:999.
[11] Antoon MK, Koenig JL. J Polym Sci 1981;19:549.
[12] Musto P, Ragosta G, Martuscelli E, Russo P, Villano P. J Appl Polym Sci 1999;74:532.
[13] Smith E, Dent G. Modern Raman spectroscopy. Chichester, UK: Wiley; 2005.
[14] Edwards HGM. Spectra – structure correlations in Raman spectroscopy. In: Chalmers JM, Griffiths PE, editors. Handbook of vibrational spectroscopy, vol. 3. New York: Wiley; 2002. p. 1838–71.
[15] Tanaka Y, Kakiuchi H. J Appl Polym Sci 1963;7:1063.
[16] Tanaka Y, Kakiuchi H. J Appl Polym Sci 1963;7:1951.
[17] Musto P, Martuscelli E, Ragosta G, Russo P. High Perform Polym 2000; 12:155.
[18] Musto P. Macromolecules 2003;36:3210.
[19] Musto P, Ragosta G, Russo P, Mascia L. Macromol Chem Phys 2001; 202:3445.
[20] Gulino D, Galy J, Pascault JP. Makromol Chem 1984;185:297.
[21] Pimentel GC, McClellan AL. The hydrogen bond. San Francisco, USA: W.H. Freeman and Co. Publishers; 1960.
[22] Murthy ASN, Rao CNR. Appl Spectrosc Rev 1968;2(1):69.
[23] Antoon MK, Koenig JL, Serafini T. J Polym Sci Polym Phys Ed 1981;19: 1567.
[24] Mensitieri G, Musto P, Ragosta G. Polymer 2006;47:801.
[25] Cotugno S, Mensitieri G, Musto P, Sanguigno L. Macromolecules 2005; 38:801.
[26] Masaki S, Mitsukazu O, Hiroshi I. J Polym Sci Polym Phys Ed 1984;22: 1461.
[27] Cuddihy EF, Moacanin J. J Polym Sci Part A2 1970;8:1627.
[28] Chung HL, Kenneth AH, William WW. Br Polym J 1986;18:316.
[29] De Nograro FF, Liano-Ponte R, Mondragon I. Polymer 1996;37: 1589.
[30] Heux L, Halary JL, Laupretre F, Monnerie L. Polymer 1997;38:1767.
[31] Starkweather HWJ. Polymer 1991;32:2443.
[32] Starkweather HWJ. Macromolecules 1990;23:328.
[33] Cukierman S, Halary JL, Monnerie LJ. Polym Eng Sci 1991;31:1476.
[34] Tobolski AV. Properties and structure of polymers. New York: J. Wiley; 1960.
[35] Williams ML, Landell RF, Ferry JD. J Am Chem Soc 1955;77:3701.
[36] Ferry JD. Viscoelastic properties of polymers. New York: J. Wiley; 1980.